fire

MDPI

Article

Characterization of Medium-Scale Accidental Releases of LNG

Paolo Mocellin [1], Gianmaria Pio [2,*], Mattia Carboni [1], Francesco Pilo [3], Chiara Vianello [1,4] and Ernesto Salzano [2]

[1] Department of Industrial Engineering, University of Padova, Via Marzolo 9, 35131 Padova, Italy; paolo.mocellin@unipd.it (P.M.); chiara.vianello@unipd.it (C.V.)
[2] Department of Civil, Chemical, Environmental, and Materials Engineering, University of Bologna, Via Terracini 28, 40131 Bologna, Italy; ernesto.salzano@unibo.it
[3] Italian National Fire and Rescue Service, Via Motorizzazione 7, 37100 Venezia, Italy; francesco.pilo@vigilfuoco.it
[4] Department of Civil, Environmental and Architectural Engineering, University of Padova, Via Marzolo 9, 35131 Padova, Italy
* Correspondence: gianmaria.pio@unibo.it

Abstract: The need for sustainable energy sources has recently promoted the use of liquefied natural gas (LNG) as a low-carbon fuel. Although economic evaluations indicate the transportation of LNG as a convenient solution for long distances between markets and reservoirs, several concerns are still present regarding its safe use and transportation. The preliminary evaluations performed in this work indicate that credible releases deriving from real bunkering operations result in pools having a diameter smaller than 1 m, which has been poorly investigated so far. Hence, an experimental campaign devoted to the characterization of a medium-scale release of LNG was carried out either in the presence or absence of an ignition source. An evaporation rate of 0.005 kg s^{-1} m^{-2} was collected for the non-reactive scenario, whereas the measured burning rate was 0.100 kg s^{-1} m^{-2}. The reduction factor of 20 demonstrates the inaccuracy in the commonly adopted assumption of equality between these values for the LNG pool. Flame morphology was characterized quantitatively and qualitatively, showing a maximum ratio between flame height and flame diameter equal to 2.5 and temperatures up to 1100 K in the proximity of the flame.

Keywords: liquefied natural gas; evaporation rate; burning rate; pool fire; safety

Citation: Mocellin, P.; Pio, G.; Carboni, M.; Pilo, F.; Vianello, C.; Salzano, E. Characterization of Medium-Scale Accidental Releases of LNG. *Fire* **2023**, *6*, 257. https://doi.org/10.3390/fire6070257

Academic Editors: Depeng Kong, Anthony Hamins and Chen Jian

Received: 18 May 2023
Revised: 15 June 2023
Accepted: 26 June 2023
Published: 30 June 2023

1. Introduction

The use of natural gas has recently been boosted by technical, environmental, economic, and political factors [1,2]. Indeed, natural gas is widely recognized as one of the most sustainable alternatives among fossil fuels for sustainable development [3–5]. In addition, natural gas can be conveniently considered a short-term solution for the energy transition, especially for hard-to-abate sectors such as trucks and ships. Regarding the storage and transportation alternatives, cryogenically liquefied natural gas (LNG) can be preferred to compressed natural gas (CNG) in case of long distances between reservoirs and markets or the absence of a suitable level of infrastructure. The increasing diffusion of LNG should be coupled with an accurate assessment of safety aspects based on an in-depth characterization of phenomenological aspects ruling the accidental release [6,7]. Particular attention should be posed to the interactions between cryogenic systems and the atmosphere [8,9] in the case of an accidental release on the ground or in water due to failure of the containment system (pipe, hose, or tank) or during the loading/unloading operations [10,11]. According to the literature and technical regulations, any accidental release of LNG can lead to several scenarios, including pool fire, flash fire, and jet fire, based on the presence of immediate or delayed ignition or just the atmospheric dispersion [12]. Due to its likelihood and its potential to trigger domino effects and have consequences for human beings in close surroundings [13], pool fires are of particular interest [14–16].

Regardless of the flammable liquid material and substrate where the release occurs, pool fires are typically characterized by three phases: initiation, pseudo-steady state, and termination. The first phase is related to the formation of fire above the pool, and it is characterized by an increased burning rate over time, resulting in a larger heat release rate. In the second phase, the presence of a stable flame can be observed. It can be fairly described as a cylinder tilted by the wind (Figure 1), thus with an almost constant mass burning rate. The third phase is associated with a reduction of flame size and mass burning rate due to the limited amount of fuel forming the liquid pool. A representation of the flame can be obtained by considering the flame dimensions (diameter D_f, height H_f, length L_f, and area A_f) and the tilt angle (δ). Quite obviously, atmospheric conditions can play a relevant role in the determination of flame geometry. Among the others, wind speed and direction represent the most influential parameters on pool fires [17]. In this sense, dedicated analysis based on laboratory scale tests is recommended to produce a stable and controlled atmosphere suitable for the realization of dedicated models. Examples of this approach can be found in the recently published literature [18]. Nevertheless, practical knowledge can be gathered utilizing on-field tests, as well as being a possible representation of a credible scenario of an accidental release in the atmosphere.

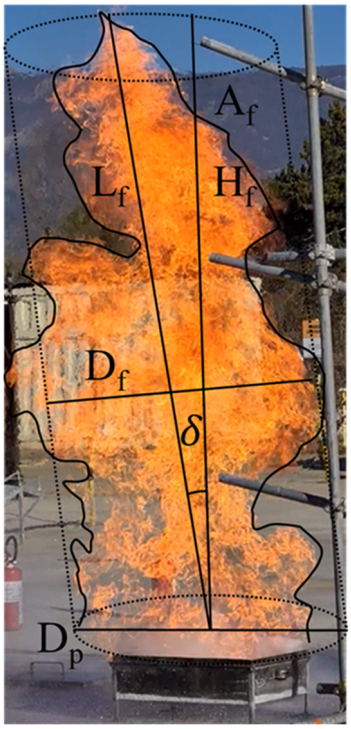

Figure 1. Overview of main parameters for the description of flame morphology on a picture representative of a pool fire produced in the experimental campaign conducted in this work.

If the accidental release is unbounded, a circular pool having a diameter variating with time from the release can be formed until a steady state is reached [19]. Alternatively, a rectangular shape can be expected for non-movable industrial installation, where a catch basin is commonly used to collect the liquid spill. In this case, an equivalent diameter can be assumed for the sake of simplicity. Usually, the flame diameter D_f is supposed to be equal to D_p. In addition, the flame height H_f can be estimated using the mass burning rate per unit area (m''). Several correlations have been proposed for this aim, as reviewed by Raj [20], including the pioneering study performed by Thomas [21], leading to the homonymous correlation. The parameter m'' is typically employed to represent the consumption rate of the pool due to the combustion, whereas the evaporation rate per unit area (m''_{ev}) represents the homologous parameter in the absence of an ignition source, i.e., the net phase change per unit area from a liquid pool to the atmosphere. It should be noted

that in a complex processing facility, there is the likelihood of the occurrence of cascading scenarios, i.e., hydrocarbon release, fire, explosion, and dispersion of combustion products. It has empirically been proven that both properties can be significantly affected by the consequences generated by the release of liquid fuels [22]. This is particularly relevant for medium- and small-scale releases. Indeed, Babrauskas et al. [23] have proposed ~ 5 m as the infinite diameter of LNG (D_∞), namely, the minimum diameter where the asymptotic value of burning rate per unit area (m''_∞) can be achieved. According to this model, the following equation is currently adopted for the definition of m'':

$$m'' = m''_\infty \cdot \left(1 - e^{-k\beta D_p}\right) \quad (1)$$

where k and β are empirical factors that depend on the investigated fuel. Specifically, k is the absorption-extinction coefficient, which is approximately 3.0 m^{-1} for LNG [24], and β is the correction coefficient for the beam length. Most of the reported values for $k\beta$ range between 0.14 m^{-1} and 0.46 m^{-1}. Although more recent studies have reported different trends for the mass burning rate per unit area, a consensus in the scientific community on the effects of pool diameter on this parameter has been achieved [25]. Starting from the '70s, several tests focused on increasing knowledge of accidental scenarios of LNG were conducted [20]. These tests considered either reactive (i.e., pool fire) or non-reactive (i.e., pool evaporation) scenarios deriving from different pool sizes up to 35 m. A collection of these data is reported in Table 1. A significant discrepancy can be observed among the different sources, although similar investigated conditions were reported at this stage [23]. Similar conclusions could be drawn for the L_f/D_p ratios reported so far. Moreover, comparable values for m'' and m''_{ev} are reported, despite the differences in the boundary conditions characterizing the system from a thermal point of view. As it is possible to note, the majority of data have been collected for $D_p > 5$ m (i.e., larger than D_∞), whereas a dearth of studies can be observed for $D_p < 1$ m. Generally speaking, even if large-scale experimental scenarios have already been tested [26] and modelled [27], quite unexpectedly, small- and medium-scale experiments are rare, as recently observed also by Zhang et al. (2018) [28]. To this aim, data on the mass evolution over time can be conveniently integrated by qualitative (e.g., images) and quantitative (e.g., thermocouples and pyrometers) analyses on the thermal aspects in the proximity of a pool fire [29]. The construction of a comprehensive database including these scales can be valuable for the evaluation and comparison of different numerical approaches, such as computational fluid dynamics [30]. Furthermore, soot data are almost absent for the analysed compounds [31] and are lacking for medium scale [32], promoting the implementation of a dedicated experimental campaign [33]. In this sense, the analysis of the most relevant reactions ruling the overall reactivity and the formation of by-products at low-temperature is paramount [34].

Table 1. Overview of the main characteristics of selected experimental campaigns on the accidental release of LNG from the literature.

Scenario	Diameter	Results	Reference	Year
Pool fire on water	15	m'' = 0.180 *; 0.495 * kg s^{-1} m^{-2} L_f/D_p = 2.8; 4.4	[31,35]	1979
	30	L_f/D_p = 2.6	[36,37]	1980
Pool fire on insulated concrete	20	L_f/D_p = 2.15 m'' = 0.106 kg s^{-1} m^{-2}	[38]	1982
	1.13 **	L_f/D_p = 3.54 m'' = 0.065 kg s^{-1} m^{-2}	[39]	2011

Table 1. *Cont.*

Scenario	Diameter	Results	Reference	Year
Pool fire on soil	35	L_f/D_p = 2.2 m'' = 0.140 kg s^{-1} m^{-2}	[40]	1989
	1.8, 6.1	L_f/D_p ϵ [1.84—3.05] m'' ϵ [0.052—0.104] kg s^{-1} m^{-2}	[41]	1974
	7.4 **	m'' = 0.054 kg s^{-1} m^{-2}	[42,43]	1984
Pool evaporationon water (no fire)	1.97, 3.63	m'' = 0.029 kg s^{-1} m^{-2}	[44]	1973
	0.75, 6.06	m'' = 0.181 kg s^{-1} m^{-2}	[45,46]	1970
	7, 14	m'' = 0.195 kg s^{-1} m^{-2}	[47,48]	1972
	10	m'' = 0.085 kg s^{-1} m^{-2}	[49,50]	1982
	6.82, 7.22	m'' = 0.120 kg s^{-1} m^{-2}	[51]	1978
Trench fire	0.22—6.8	m'' ϵ [0.022—0.13] kg s^{-1} m^{-2}	[23]	1983

* Calculated considering a density of 450 kg m^{-3}. ** Equivalent diameter.

Under these premises, the identification of the sizes representative of credible accidental releases of LNG is an essential step from the safety and risk engineering perspective. In this sense, the accidental release of LNG during bunkering operation has been largely considered one of the most critical phases [6], taking into account their elevated likelihood to occur [52]. Furthermore, the transportation and bunkering processes are concerns of public authorities and the population [53,54], having the potential to generate vapour dispersion and pool fires [53]. To this aim, loading arms and flexible hoses are mentioned as typical transfer systems in the specific literature [6]. Hence, leak diameters varying from 5 to 20 mm, as well as a fully automatic emergency shutdown system, are considered; thus, a release of 30 s can be assumed and modelled following the current literature [55,56]. The full set of results is reported in the Supplementary Material (Table S1). However, it is worth noting that maximum D_p of 0.80 m and 1.40 m were obtained for release on the ground and water, respectively.

In this light, the experimental campaign reported in this work aimed to characterize reactive and non-reactive scenarios of small/medium scale (i.e., $D_p < 1$), which are most representative of common processes employed during bunkering or transfer of the fuel. Indeed, the collected measurements represent an essential database for the validation or modification of the existing models in the case of medium-scale accidental releases of LNG in poorly congested areas. The determination of mass burning rate and flame geometry in on-field tests can also be intended as a paramount step for the optimization of emergency response plans, since the gathered information also accounts for the possible spatial and temporal oscillations of the boundary conditions.

2. Methodology

The experimental tests reported in this work were conducted in collaboration with the Nuclear Biological Chemical and Radiological (NBCR) team of the Italian National Fire and Rescue Service (Minister of Interior). Either reactive or non-reactive scenarios resulting from an accidental release of LNG were tested in an on-field environment. The LNG was composed essentially of methane (89.48%v), ethane (8.76%v), propane (1.16%v), nitrogen (0.50%v), and a low amount of butane. The initial composition of the adopted LNG results in a density equal to 453.5 kg m^{-3} at a temperature of −160 °C. A preliminary investigation was devoted to the characterization of the most representative size for a credible accidental release of LNG. Based on the composition and boundary conditions of interests, the accidental release of LNG during bunkering operation (considered one of the most critical phases [6]) was characterized via state-of-art models [56]. To this aim, a vertical jet directed on the ground, wind velocity of 5 m s^{-1}, a neutral (D) stability class, a release of 30 s (i.e., a fully automatic emergency shutdown system was considered), and typical transfer systems were reported in the specific literature [6], and leak diameters of varying

from 3 to 6 mm were assumed, following the values recommended by the literature [55]. The results of these calculations are reported in Table 2.

Table 2. Estimation of pool dimensions in case of an accidental release of LNG during bunkering operations.

Transfer System	Size [in]	Pressure (*P*) [bar]	Substrate	Pool Diameter (D_p) [m]	Mass (*m*) [kg]
Loading arm	6	5.55	Concrete	0.80	8.4
			Water	1.40	5.4
Loading arm	12	7.55	Concrete	0.44	1.95
			Water	0.89	2.38
Flexible hose	2	12.0	Concrete	0.35	2.55
			Water	0.75	3.34

Under these assumptions, D_p is lower than 0.80 m in case of release on the ground and lower than 1.40 m for a release in water. Hence, the majority of experimental campaigns available in the current literature explore larger scenarios, possibly not representative of the bunkering operations. In this light, the experimental campaign reported in the following aimed to characterize reactive and non-reactive scenarios of small/medium scale (i.e., $D_p < 1$).

For all tests, the temperature field developed in the proximity of the cryogenic pool was measured by an arrangement of type-K thermocouples with an estimated accuracy of ±2.5 °C [57]. The acquisition rate variated between 6 and 30 samples per minute. In addition, visible and infrared (IR) digital images were recorded during the tests. A FLIR thermal imaging camera (model T1010) with an accuracy of ±2 °C and a frame rate of 30 Hz was employed at this scope. Using thermal and visible images, the flame characteristics (H_f, D_f, A_f, and δ) were analysed for the reactive scenarios. Furthermore, the burning rate per unit area (m''_{ev}) was evaluated for the fire tests by assessing the liquid level evolution over time. For m'', data were filtered to remove noise and irregularities using a 100 points Savitzky–Golay (SG) method. The experimental procedure was designed to reduce the variability of atmospheric parameters within each test. However, small oscillations were observed (within 5% of the average value). For the sake of simplicity, only the average ambient conditions are reported in terms of wind velocity (u_w) and direction, ambient temperature (T_a), and relative humidity (Table 3).

Table 3. Ambient conditions registered during the tests.

Test #	Ambient Temperature (T_a) [°C]	Humidity [%]	Wind Velocity (u_w) [m s^{-1}]	Wind Direction [°]
Test A	6.6	32	0.7	96
Test B	3.7	44	0.5	322
Test C	7.0	32	1.0	286
Test D	7.2	31	1.7	22
Test E	6.9	31	1.4	307

2.1. Dispersion Test

For the dispersion tests, a steel rectangular-shaped drip tray with dimensions of 0.750 m · 0.485 m · 0.011 m was employed. Hence, an equivalent diameter (D_p) of 0.68 m was considered. This diameter has also been chosen for pool fire, as reported below, based on a preliminary evaluation obtained using integral models [56]. Additional details are reported in the Design of Experiment section of the Supplementary Material.

The mass evolution over time was measured using a load cell with a capacity of 60 kg and a resolution of 20 g. Values were acquired with a frequency of 0.1 Hz. Consequently, using the geometrical characteristic of the drip tray, the evaporation rate per unit area (m''_{ev})

was calculated as the first derivative of the measured mass divided by the liquid–vapour interface at any given time.

2.2. Pool Fire

The pool fire tests were conducted employing the same drip tray (D_p ~ 0.68 m) for the sake of comparison with the non-reactive scenario (i.e., dispersion). The relative position of the adopted thermocouples is given in Table 4, where the coordinates are expressed as x, y, and z, with the origin coinciding with the centre of the drip tray. More specifically, the positions referred to as V_i are located on the axis of symmetry of the adopted box, whereas the points reported as H_i are located at z equal to 2 m and horizontally distanced by 1 m each from the edge of the box. Further information on this aspect can be retrieved in the previously published literature [58]. In addition, IR images were collected during the experimental campaign to quantify the main geometrical characteristics of the undetached plume.

Table 4. Position of thermocouples adopted for the characterization of temperature distribution from pool fire tests expressed (x, y, z) coordinates considering the centre of the drip tray as the origin.

	V1	V2	V3	V4	H5	H6	H7	H8
x [m]	0	0	0	0	0.375	1.375	2.375	3.375
y [m]	0	0	0	0	0	0	0	0
z [m]	4	3	2	1	2	2	2	2

3. Results and Discussion

In the following sections, the results of the experiments are presented. First, the results obtained by the evaporation test (Test A) are reported and discussed. Then, pool fire scenarios are analysed and compared with the non-reactive scenario and data from the current literature.

3.1. Evaporation

In Test A, a quantity of 8.68 kg of LNG was spilt in the drip tray, and the non-reactive scenario was investigated using the load cell (Figure 2).

Figure 2. Evaporation of cryogenic liquid released in the atmosphere, as observed in Test A.

Figure 3 shows the mass profile (m) and the evaporation rate (m''_{ev}) as a function of time.

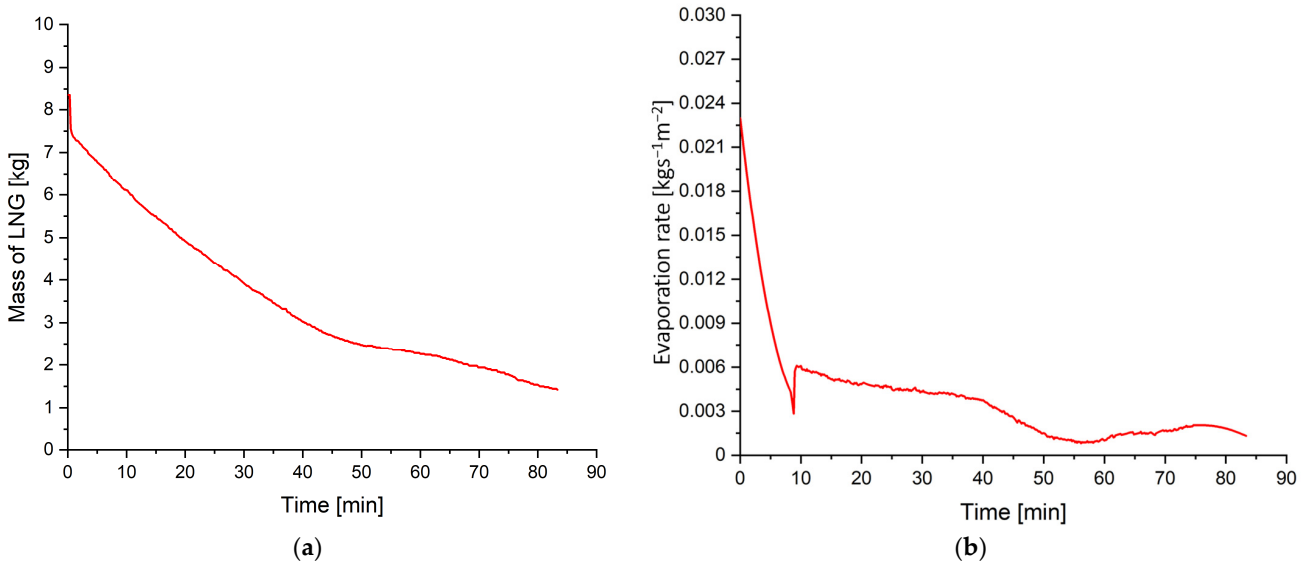

Figure 3. Mass profile (**a**) and evaporation rate m''_{ev} (**b**) with respect to time.

From a phenomenological point of view, in the first part of the test, a peak in m''_{ev} is observed. Indeed, a maximum value equal to 0.023 kg s^{-1} m^{-2} is obtained at the very beginning of the experiment.

The initial peak can be attributed to two factors. The first is driven by the mass transfer and is related to the initial absence or limited presence of a vapour cloud in the proximity of the liquid–gas interface that brings a reduction in the effect of the condensation term in the net evaporation rate. Indeed, several theories, including the well-known Lee's model [59], account for the contribution of two phenomena to the net evaporation rate: condensation of vapour particles in the proximity of the liquid–vapour interface and evaporation of liquid particles in the proximity of the liquid–vapour interface. The second is driven by the contribution of heat exchange by conduction, which becomes negligible in the stationary phase. In this regard, detailed discussions on the effects of the initial wetting and cool-down of the containing vessel on the evaporation rate of cryogenic liquids can be found in the literature [60]. Quite obviously, this aspect is potentially largely affected by the thermal properties of the substrate considered in the analysis. Indeed, a large share of the heat exchange between cryogenic liquids and the surrounding environment is typically attributed to the conductive term [61]. Afterwards, a linear decrease of liquid mass representative of a stationary phase can be observed. As a result, a m''_{ev} value of 0.005 kg s^{-1} m^{-2} is obtained. This trend can be associated with the achievement of an equilibrium phase between the evaporation and condensation terms; thus, it is reached as soon as a stable layer is formed. This phase lasts approximately 40:00 min. After this phase, a slowing in evaporation is registered due to the consumption of most of the initial mass, enrichment in heavier species in the liquid pool, and reduction in driving forces ruling the evaporation term.

The value acquired in Test A is significantly lower than the m''_{ev} reported in the literature, even though a more conductive substrate was utilized in this work. Indeed, according to Luketa-Hanlin et al. (2006) [44], the mass evaporation rate m''_{ev} can vary between 0.029 kg s^{-1} m^{-2} and 0.195 kg s^{-1} m^{-2}. In addition, several numerical studies have adopted 0.181 kg s^{-1} m^{-2} as a reference value, following a conservative approach [62]. The difference between data collected in this work and retrieved in the literature can be mainly attributed to the adopted substrate and pool size. Indeed, it should be noted that most of the evaporation data from the literature were acquired employing water or soil as a substrate [45,47–50,52]. Hence, a correction factor between two and three is recommended to correlate water and land evaporation rates [63] to account for the differences in heat

transfer from the substrate to the cryogenic pool. As a way of example, DNV PHAST uses a factor of 2.5, as reported in Equation (2) [64]:

$$m''_{ev,water} \approx 2.5 \cdot m''_{ev} \quad (2)$$

3.2. Pool Fire

Four tests were performed for the pool fire scenario (Test B–E). In Test B, 16.5 kg of LNG was spilled into the drip tray and consequently ignited. The test lasted 8 min. An initial growing phase was detected within the first 10 s after the ignition, as can be observed in Figure S6 included in the Supplementary Materials, followed by a pseudo-steady state where reduced oscillations are reported for each geometrical feature of the produced flame. Due to the wind effect, the flame was tilted for almost the entire experiment duration, so the thermocouples were rarely enveloped by the flame (Figure 4).

Figure 4. Flame tilted by the wind as obtained during Test B.

It should be noted that the formation of black, solid particles (i.e., soot) cannot be observed in the upper part of the flame. This observation is particularly remarkable if the sooting tendency of LNG pool fire reported in the literature is analysed. More specifically, field experiments reported by Suardin et al. (2011) [65] show light and clear flame, whereas a significant formation of soot particles has been observed by Luketa and Blanchat (2015) [66]. Although the liquid composition is unquestionably a potential factor for the soot formation, and these values are not available for all the cited cases, large differences in soot tendency cannot be associated only with the composition since the variations are constrained by dedicated standards [67]. The main difference between the abovementioned experimental campaigns relies on the size of the investigated pool, namely, in the first case, a medium scale has been investigated. In contrast, a large scale has been tested in the latter case. Typically, the formation of carbonaceous particles in pool fires has been attributed to low mixing levels in the core area, which generates a possible dearth of fuel vapour or oxygen content for the oxidation of pyrolysis products [31]. The comparison of the obtained results with data from the literature demonstrates that this condition can be related either to the pool diameter or the addition of diluents (e.g., water, nitrogen, and carbon dioxide). In the former case, the temperature and concentration profile within the flame may locally generate conditions promoting the formation of soot, whereas in the latter case, the formation of soot particles can also be attributed to modifications

in the reaction pathways either due to a direct or indirect role of diluent agents. More specifically, the presence of a diluent can modify the reaction rates of activation steps at low temperatures (i.e., hydrogen abstraction) by affecting the availability of typical abstracting agents (e.g., OH, H, and O) [68,69], with significant impacts on the associated branching ratios. This phenomenon can be ascribed to a direct role. Conversely, the indirect role of diluents can be related to chemical dilution (i.e., decrease in the concentration of reactants), physical dilution (i.e., heat sink action), or effective collisions (i.e., promotion of termination reactions as third body agents).

Due to the wind direction and the relative position between thermocouples and the pool, the measured temperature has never exceeded the value of 180 °C, registered 1 m above the drip tray (Figure 5). Similar data collected for different tests are reported in Figures S3 and S5.

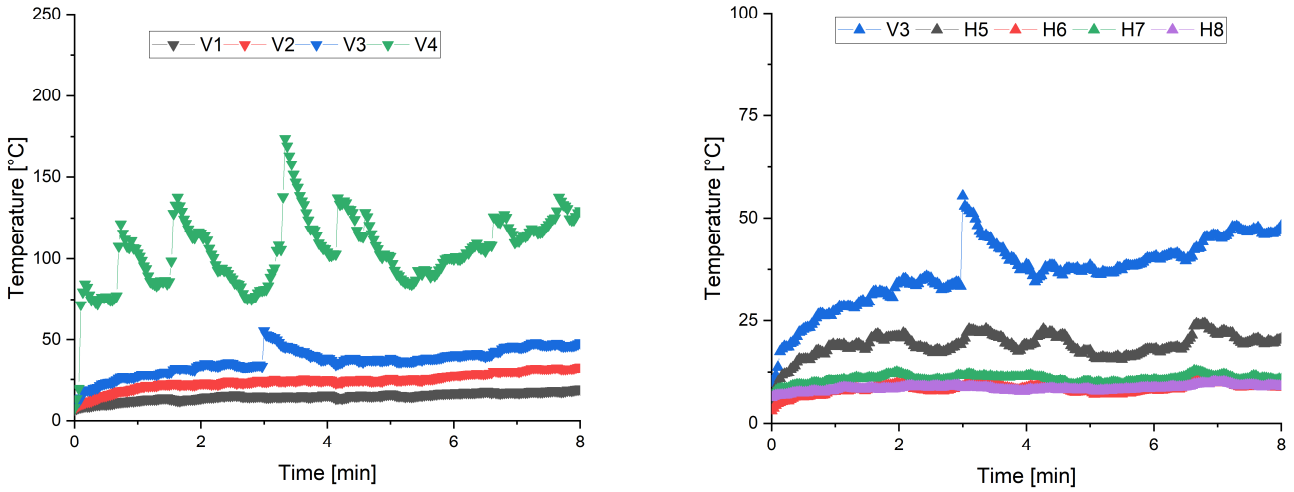

(**a**) (**b**)

Figure 5. Vertical (**a**) and horizontal (**b**) temperature profiles as a function of time obtained during Test B.

Along with the horizontal profile, the recorded temperature value was always lower than 50 °C (Figure 5b). This is particularly relevant if the corresponding radiative flux is calculated. Indeed, under the conservative assumptions posed by the Stefan–Boltzmann law, the corresponding maximum heat flux (q_{max}) is lower than 2.4 kW m^{-2} (the thermal radiation required to generate a 2nd-degree burn [70]). On the other hand, if the IR images are considered (Figure 6), temperatures up to 650 °C can be observed in a position not covered by the thermocouples, corresponding to q_{max} equal to 41 kW m^{-2}, which can turn out in domino scenarios [71]. In addition, a structure characterized by three areas can be identified. More specifically, a cold pocket in the proximity of the pool, followed by the core combustion-driven area, where maximum temperatures are reached, and hot gas diffusion can be observed. These results demonstrate that the wind direction strongly affects the produced flame and the resulting area of concern.

For the sake of brevity, temperature, IR images, and temperature profiles measured for Test C, Test D and Test E were reported in Figures S1, S2, and S4 included in the Supplementary Materials. Starting from the visible features of the flames collected in this work, morphology data of the different tests were collected every 20 s. The minimum, average, and maximum values for the main characteristics of the flame are provided in Table 5. Generally speaking, starting from these data, it is possible to conclude that an LNG pool of $D_p \sim 1$ burns at the average rate of 0.100 kg s^{-1} m^{-2} and produces a flame height of 1.6 m with a diameter roughly equal to the diameter of the pool at a maximum temperature of 800 °C at which corresponds a q_{max} equal to 75 kW m^{-2}, which can lead to domino effects for pressurized tanks [71]. Regarding the burning rates, it is possible to

affirm that, except for Test B, values are in the range of 0.093 to 0.119 kg s^{-1} m^{-2}. This is in good agreement with the literature data [23,36,41,42]. In addition, it is possible to note that m'' of Test B is more than half that of other tests. Indeed, due to the wind effect, the flame was tilted. This caused a worse heat exchange between the proximity of the free surface of the pool and the flame. The result is that m'' assumes an intermediate value between burning and evaporation rates. Regarding L_f/D_p, except for Test B, a range varying between 2.0 and 2.5 could be roughly identifiable, which is in line with values reported in the current literature [35,39,41].

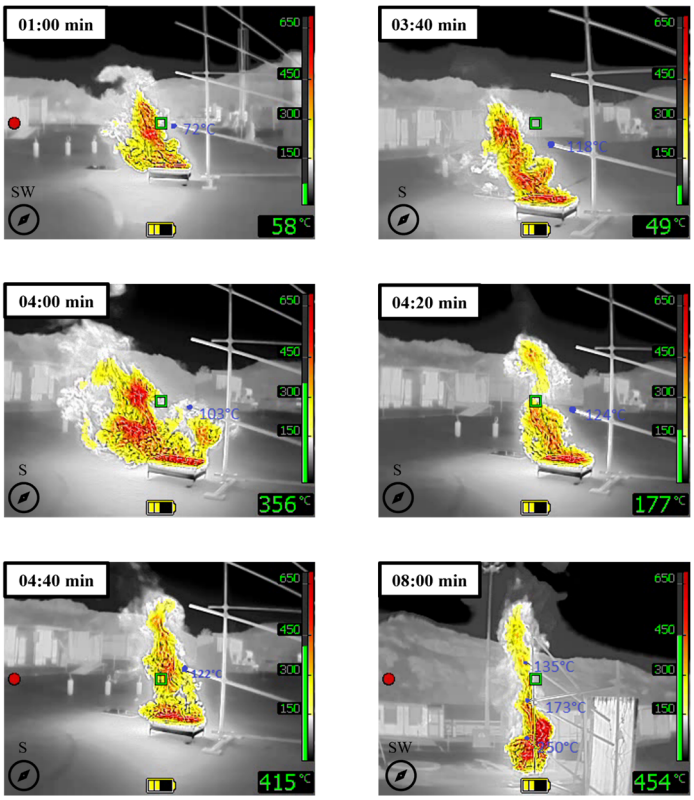

Figure 6. Infrared images collected during Test B. For the sake of comparison, temperature values collected by thermocouples were added. Values reported on the bottom right side of each panel refer to the points indicated by the green square located on the flame surface.

Table 5. Flame morphology characteristics (Figure 1) measured during different tests carried out in this work.

		H_f [m]	D_f [m]	A_f [m]	$\|\delta\|$ [°]	m'' [kg s^{-1} m^{-2}]	T [°C] (# Thermocouple)
Test B	Max	1.68	1.13	1.09	55	0.042	173 (V4)
	Average	1.06	0.71	0.63	33		-
	Min	0.61	0.46	0.29	3		-
Test C	Max	2.39	1.31	1.88	42	0.093	780 (V4)
	Average	1.59	0.85	1.15	13		-
	Min	0.59	0.53	0.48	0		-
Test D	Max	2.43	1.00	1.20	50	0.119	780 (V4)
	Average	1.39	0.62	0.54	12		-
	Min	0.31	0.23	0.01	1		-
Test E	Max	2.43	0.96	1.29	19	0.099	790 (V4)
	Average	1.62	0.57	0.70	6		-
	Min	0.35	0.14	0.03	0		-

The mass burning rate values were compared with the evaporation rate collected in this work and reported in the previous section. It is possible to conclude that a factor of 20 should be considered to switch between a non-reactive to reactive scenario (Equation (3)):

$$m'' \approx 20 \cdot m''_{ev} \quad (3)$$

Indeed, during a pool fire, the heat from the fire normally radiates back into the pool, generating the vapour that burns in a quasi-steady state. Hence, increased efficiency of the heat exchange is expected. When pool fires are on soil or ground, a negligible amount of heat is transferred by conduction [64]. In addition, it should be noted that the difference between m'' and m''_{ev} evaluated in this work is considerably higher than the literature values.

The suggested modifications in the evaporation rate and mass burning rate associated with a medium-scale pool fire of LNG can significantly impact the consequence analysis of the corresponding scenarios. Regardless of the analysed scenario, the duration to be considered in the analysis shall be extended for any initial quantity of released LNG.

Concerning the consequence, the reduction of the mass burning rate results in smaller emissive power, under the reasonable assumption that the fraction of energy radiated by the fire and the heat of combustion are constant [72]. Hence, the stand-off distances for pool fire of LNG shall be reconsidered based on a more accurate mass burning rate. Concerning the non-reactive scenario, a decrease in evaporation rate limits the occurrence of a rapid phase transition [73] and affects the design of mitigation systems [74].

4. Conclusions

In this work, evaporation tests and pool fires of liquefied natural gas (LNG) were performed in a drip tray, representative of a credible release during typical bunkering operations. The pool evaporation, in the case of the absence of ignition sources, has shown a rate value that is about 0.005 kg s^{-1} m^{-2}, which is considerably lower than the value typically assumed for numerical analysis and approximately 20 times lower than the measured mass burning rate, which indeed was estimated as 0.100 kg s^{-1} m^{-2}. Quantitative and qualitative information gathered throughout the experimental campaign described in this work were utilized to characterize the flame geometry resulting from an LNG pool fire.

Supplementary Materials: The following supporting information can be downloaded at https://www.mdpi.com/article/10.3390/fire6070257/s1. Table S1: Results of the estimation of pool dimensions in case of an accidental release of LNG during bunkering operations. Figure S1: IR images of TEST C. Temperatures reported inside the image refer to thermocouple's values. Values reported on the right bottom side of each panel refer to the area within the green region. Figure S2: IR images of TEST D. Temperatures reported inside the image refer to thermocouple's values. Values reported on the right bottom side of each panel refer to the area within the green region. Figure S3: Vertical (a) and horizontal (b) temperature profile versus time of TEST D. Figure S4: IR images of TEST E. Temperatures reported inside the image refer to thermocouple's values. Values reported on the right bottom side of each panel refer to the area within the green region. Figure S5: Vertical (a) and horizontal (b) temperature profile versus time of TEST E. Figure S6: Geometrical characteristics of pool fire experimental tests retrieved from visible images acquired every 20 s.

Author Contributions: Conceptualization, P.M. and G.P.; methodology, P.M. and M.C.; software, P.M. and G.P.; validation, P.M., M.C., and F.P.; formal analysis, P.M., G.P., and M.C.; investigation, P.M., M.C., and F.P.; resources, F.P., C.V., and E.S.; data curation, P.M. and G.P.; writing—original draft preparation, P.M. and M.C.; writing—review and editing, P.M., G.P., C.V., and E.S.; visualization, P.M., G.P., and M.C.; supervision, C.V. and E.S.; project administration, E.S.; funding acquisition, C.V. and E.S. All authors have read and agreed to the published version of the manuscript.

Funding: This research was funded by Adriatic-Ionian Program INTERREG V-B Transnational 2014–2020, project # 1267- SUPER-LNG PLUS.

Institutional Review Board Statement: Not applicable.

Informed Consent Statement: Not applicable.

Data Availability Statement: Data is contained within the article or supplementary material.

Acknowledgments: The authors gratefully acknowledge the contribution made by Alessandro Zanetti (Nuclear Biological Chemical and Radiological (NBCR) team of the CNVVF Italian National Fire and Rescue Service) and his team.

Conflicts of Interest: The authors declare no conflict of interest.

Nomenclature

Symbol	Definition	Symbol	Definition
k	Absorption-extinction coefficient	L_f	Flame length
T_a	Ambient temperature	m''	Mass burning rate per unit area
β	Correction for beam length	m''_∞	Mass burning rate per unit area for large pools
m''_{ev}	Evaporation rate per unit area	D_p	Pool diameter
A_f	Flame area	δ	Tilt angle
D_f	Flame diameter	u_w	Wind speed
H_f	Flame height		

References

1. Chen, Z.; Zhang, F.; Xu, B.; Zhang, Q.; Liu, J. Influence of methane content on a LNG heavy-duty engine with high compression ratio. *Energy* **2017**, *128*, 329–336. [CrossRef]
2. Osorio-Tejada, J.L.; Llera-Sastresa, E.; Scarpellini, S. Liquefied natural gas: Could it be a reliable option for road freight transport in the EU? *Renew. Sustain. Energy Rev.* **2017**, *71*, 785–795. [CrossRef]
3. Kalghatgi, G.; Levinsky, H.; Colket, M. Future transportation fuels. *Prog. Energy Combust. Sci.* **2018**, *69*, 103–105. [CrossRef]
4. Crippa, M.; Janssens-Maenhout, G.; Guizzardi, D.; Galmarini, S. EU effect: Exporting emission standards for vehicles through the global market economy. *J. Environ. Manag.* **2016**, *183*, 959–971. [CrossRef]
5. Yin, F.; Gangoli, A.; Bhat, A.; Chen, M. Performance assessment of a multi-fuel hybrid engine for future aircraft. *Aerosp. Sci. Technol.* **2018**, *77*, 217–227. [CrossRef]
6. Carboni, M.; Pio, G.; Mocellin, P.; Vianello, C.; Maschio, G.; Salzano, E. Accidental release in the bunkering of LNG: Phenomenological aspects and safety zone. *Ocean Eng.* **2022**, *252*, 111163. [CrossRef]
7. Carboni, M.; Pio, G.; Mocellin, P.; Vianello, C.; Maschio, G.; Salzano, E. On the flash fire of stratified cloud of liquefied natural gas. *J. Loss Prev. Process Ind.* **2022**, *75*, 104680. [CrossRef]
8. Fy, G.; Wand, J.; Yan, M. Anatomy of Tianjin Port Fire and Explosion: Process and Caused. *Proc. Saf. Prog.* **2016**, *35*, 216–220.
9. Mocellin, P.; Vianello, C.; Maschio, G. Facing emerging risks in carbon sequestration networks. A comprehensive source modelling approach. *Chem. Eng. Trans.* **2018**, *67*, 295–300.
10. Chang, Y.T.; Park, H. The impact of vessel speed reduction on port accidents. *Accid. Anal. Prev.* **2019**, *123*, 422–432. [CrossRef]
11. Aneziris, O.; Koromila, I.; Nivolianitou, Z. A systematic literature review on LNG safety at ports. *Saf. Sci.* **2020**, *124*, 104595. [CrossRef]
12. Pio, G.; Salzano, E. The effect of ultra-low temperature on the flammability limits of a methane/air/diluent mixtures. *J. Hazard. Mater.* **2019**, *362*, 224–229. [CrossRef]
13. Masum Jujuly, M.; Rahman, A.; Ahmed, S.; Khan, F. LNG pool fire simulation for domino effect analysis. *Reliab. Eng. Syst. Saf.* **2015**, *143*, 19–29. [CrossRef]
14. Casal, J. *Evaluation of the Effects and Consequences of Major Accidents in Industrial Plants*; Elsevier: Amsterdam, The Netherlands, 2017.
15. American Petroleum Institute. *Risk-Based Inspection Technology*; American Petroleum Institute: Washington, DC, USA, 2008.
16. Baalisampang, T.; Abbassi, R.; Garaniya, V.; Khan, F.; Dadashzadeh, M. Modelling an integrated impact of fire, explosion and combustion products during transitional events caused by an accidental release of LNG. *Process Saf. Environ. Prot.* **2019**, *128*, 259–272. [CrossRef]
17. Palacios, A.; Rengel, B. Flame shapes and thermal flux of vertical hydrocarbon flames. *Fuel* **2020**, *276*, 118046. [CrossRef]
18. Ji, J.; Li, F.; Lu, W.; Sun, R.; Wang, K.; Cao, Y. An experimental study on flame geometry in wind-blown pool fires and a new dimensionless parameter. *Case Stud. Therm. Eng.* **2022**, *30*, 101782. [CrossRef]
19. Betteridge, S. Modelling large LNG pool fires on water. *J. Loss Prev. Process Ind.* **2018**, *56*, 46–56. [CrossRef]
20. Raj, P.K. LNG fires: A review of experimental results, models and hazard prediction challenges. *J. Hazard. Mater.* **2007**, *140*, 444–464. [CrossRef]
21. Thomas, P.H. The size of flames from natural fires. *Symp. Int. Combust.* **1963**, *9*, 844–859. [CrossRef]
22. Hottel, H.C.; Noble, J.J.; Sarofim, A.F.; Silcox, G.D.; Wankat, P.C.; Knaebel, K.S. Heat and Mass Transfer. 2008. Available online: http://library.navoiy-uni.uz/files/hottel%20h.c.,%20noble%20j.j.,%20sarofim%20a.f.%20-%20perry%27s%20chemical%20engineers%27%20handbook.%20section%205%20(8th%20edition)(2008)(85s).pdf (accessed on 17 May 2023).

23. Babrauskas, V. Estimating large pool fire burning rates. *Fire Technol.* **1983**, *19*, 251–261. [CrossRef]
24. Beyler, C.L. *Industrial Fire Protection Engineering*, 1st ed.; John Wiley & Sons, Inc.: Hoboken, NJ, USA, 2004.
25. Eddings, E.G.; Yan, S.; Ciro, W.; Sarofim, A.F. Formulation of a Surrogate for the Simulation of Jet Fuel Pool Fires. *Combust. Sci. Technol.* **2005**, *177*, 715–739. [CrossRef]
26. Puttock, J.S.; Colenbrander, G.W.; Blackmore, D.R. Maplin Sands Experiments 1980: Dispersion Results from Continuous Releases of Refrigerated Liquid Propane. In Proceedings of the Heavy Gas Risk Assess—II, Frankfurt am Main, Germany, 25–26 May 1982; Springer: Dordrecht, The Netherlands, 1983.
27. Fay, J.A. Model of large pool fires. *J. Hazard. Mater.* **2006**, *136*, 219–232. [CrossRef]
28. Zhang, B.; Laboureur, D.M.; Liu, Y.; Gopalaswami, N.; Mannan, M.S. Experimental Study of a Liquefied Natural Gas Pool Fire on Land in the Field. *Ind. Eng. Chem. Res.* **2018**, *57*, 14297–14306. [CrossRef]
29. Chen, J.; Sung, K.; Wang, Z.; Tam, W.C.; Lee, K.Y.; Hamins, A. The evolving temperature field in a 1-m methanol pool fire. *J. Fire Sci.* **2021**, *39*, 309–323. [CrossRef]
30. Yang, R.; Khan, F.; Yang, M.; Kong, D.; Xu, C. A numerical fire simulation approach for effectiveness analysis of fire safety measures in floating liquefied natural gas facilities. *Ocean Eng.* **2018**, *157*, 219–233. [CrossRef]
31. Raj, P.K.; Moussa, A.; Aravamidan, K.; Messrs, P.; Von Thuna, P.; Marchessault, P.J.; Drake, E.M.; Collona, G.; Parnarouskis, M.; Schneider, A.; et al. *Experiments Involving Pool and Vapor Fires from Spills of Liquefied Natural Gas on Water*; LITTLE (ARTHUR D) Inc.: Cambridge, MA, USA, 1979.
32. Falkenstein-Smith, R.L.; Sung, K.; Hamins, A. Characterization of Medium-Scale Propane Pool Fires. *Fire Technol.* **2023**, 1–18. [CrossRef]
33. Chen, J.; Zhao, Y.; Bi, Y.; Li, C.; Kong, D.; Lu, S. Effect of initial pressure on the burning behavior of ethanol pool fire in the closed pressure vessel. *Process Saf. Environ. Prot.* **2021**, *153*, 159–166. [CrossRef]
34. Pio, G.; Salzano, E. Laminar Burning Velocity of Methane, Hydrogen and Their Mixtures at Extremely Low Temperature Conditions. *Energy Fuels* **2018**, *32*, 8830–8836. [CrossRef]
35. Schneider, A.L. Liquefied natural gas spills on water: Fire modelling. *J. Fire Flamm.* **1980**, *12*, 302–313.
36. Hirst, W.J.S.; Eyre, J.A. Maplin Sands Experiments 1980: Combustion of Large LNG and Refrigerated Liquid Propane Spills on the Sea. In Proceedings of the Heavy Gas Risk Assess—II, Frankfurt am Main, Germany, 25–26 May 1982; Hartwig, S., Ed.; Springer: Dordrecht, The Netherlands, 1983.
37. Nizner, G.A.; Eyre, J.A. Radiation From Liquefied Gas Fires On Water. *Combust. Sci. Technol.* **1983**, *35*, 33–57. [CrossRef]
38. Mizner, G.A.; Eyre, J.A. *Large-Scale LNG and LPG Pool Fires*; EFCE Publication Series; European Federation of Chemical Engineering: Frankfurt am Main, Germany, 1982.
39. Gomez, C.H. Experiments for the Measurement of LNG Mass Burning Rates. Ph.D. Thesis, Texas A & M University, College Station, TX, USA, 2011.
40. Nedelka, D.; Moorhous, J.; Trucker, R.F. The Montoir 35m diameter LNG pool fire experiments. *Int. Conf. Liq. Nat. Gas.* **1989**, *2*. Available online: https://www.google.pt/books/edition/The_Montoir_35m_Diameter_LNG_Pool_Fire_E/J3q8HAAACAAJ?hl=it (accessed on 17 May 2023).
41. American Gas Association. *LNG Safety Program: Interim Report on Phase II Work*; Project IS-3-1; American Gas Association: Columbus, OH, USA, 1974.
42. Moorhouse, J.; Croce, P.A. Thermal radiation from LNG trench fires. *Ann. Phys.* **1984**. [CrossRef]
43. Luketa-Hanlin, A. A review of large-scale LNG spills: Experiments and modeling. *J. Hazard. Mater.* **2006**, *132*, 119–140. [CrossRef]
44. Boyle, G.J.; Kneebone, A. *Laboratory Investigations into the Characteristics of LNG Spills on Water. Evaporation, Spreading and Vapor Dispersion*; Report 6-32; Shell Research Ltd., Thornton Research Centre: Thornton, UK, 1973.
45. Burgess, D.S.; Biordi, J.; Murphy, J. *Hazards Associated with the Spillage of LNG on Water*; Report 7448; Bureau of Mines: Pittsburgh, PA, USA, 1970.
46. Burgess, D.S.; Murphy, J.N.; Zabetakis, M.G. *Hazards of LNG Spillage in Marine Transportation*; SRS Report No. S4105; U.S. Department of Interior, Bureau of Mines: Pittsburgh, PA, USA, 1970.
47. Feldbauer, G.F.; Heigl, J.J.; McQueen, W.; Whipp, R.H.; May, W.G. *Spills of LNG on Water Vaporization and Downwind Drift of Combustible Mixtures*; American Petroleum Institute: Washington, DC, USA, 1972.
48. May, W.G.; McQueen, W.; Whipp, R.H. *Spills of LNG on Water, Paper 73-D-9*; Operation Section Proceedings; American Gas Association: Washington, DC, USA, 1973.
49. Puttock, J.S.; Blackmore, D.R.; Colenbrander, G.W. Field experiments on dense gas dispersion. *J. Hazard. Mater.* **1982**, *6*, 13–41. [CrossRef]
50. Colenbrander, G.W.; Puttock, J.S. Dense gas dispersion behavior experimental observations and model developments. *Fourth Int. Sym. Loss Prev. Saf.* **1983**, *90*, F66–F76.
51. Koopman, R.P. *Data and Calculations on 5m^3 LNG Spill Tests, UCRL-52976*; Lawrence Livermore Laboratory: Livermore, CA, USA, 1978.
52. Baalisampang, T.; Abbassi, R.; Garaniya, V.; Khan, F.; Dadashzadeh, M. Accidental release of Liquefied Natural Gas in a processing facility: Effect of equipment congestion level on dispersion behaviour of the flammable vapour. *J. Loss Prev. Process Ind.* **2019**, *61*, 237–248. [CrossRef]
53. Sun, B.; Guo, K.; Pareek, V.K. Hazardous consequence dynamic simulation of LNG spill on water for ship-to-ship bunkering. *Process Saf. Environ. Prot.* **2017**, *107*, 402–413. [CrossRef]

54. *ISO 20519:2017*; Ships and Marine Technology—Specification for Bunkering of Liquefied Natural Gas Fuelled Vessels. ISO: Geneva, Switzerland, 2017.
55. Society for Gas as a Marine Fuel (SGMF). *BASiL—Bunkering Area Safety Information LNG User Guide*, Version 6; Available online: https://www.sgmf.info/ (accessed on 1 February 2023).
56. Uijt de Haag, P.A.M.; Ale, B.J.M. *Purple Book—Guidelines for Quantitative Risk Assessment*; Purple Book; RIVM: Hague, The Netherlands, 2005.
57. Proust, C.; Jamois, D.; Studer, E. High pressure hydrogen fires. *Int. J. Hydrogen Energy* **2011**, *36*, 2367–2373. [CrossRef]
58. Mocellin, P.; Pio, G.; Carboni, M.; Pilo, F.; Vianello, C.; Salzano, E. On the effectiveness of mitigation strategies for cryogenic applications. *J. Loss Prev. Process Ind.* **2023**, *84*, 105123. [CrossRef]
59. Lee, W.H. *Pressure Iteration Scheme for Two-Phase Flow Modeling*, 1st ed.; Hemisphere Publishing: Washington, DC, USA, 1980.
60. Ponchaut, N.F.; Kytömaa, H.K.; Morrison, D.R.; Chernovsky, M.K. Modeling the vapor source term associated with the spill of LNG into a sump or impoundment area. *J. Loss Prev. Process Ind.* **2011**, *24*, 870–878. [CrossRef]
61. Nguyen, L.D.; Kim, M.; Choi, B. An experimental investigation of the evaporation of cryogenic-liquid-pool spreading on concrete ground. *Appl. Therm. Eng.* **2017**, *123*, 196–204. [CrossRef]
62. Gerbec, M.; Vidmar, P.; Pio, G.; Salzano, E. A comparison of dispersion models for the LNG dispersion at port of Koper, Slovenia. *Saf. Sci.* **2021**, *144*, 105467. [CrossRef]
63. Cook, J.; Woodward, J.L. A New Integrated Model for Pool Spreading, Evaporation, and Solution on Land and in Water. In Proceedings of the International Conference on Safety, Health and LP in the Oil, Chemical and Process Industries, Singapore, 15–19 February 1993.
64. Pitblado, R.M.; Baik, J.; Hughes, G.J.; Ferro, C.; Shaw, S.J. Consequences of LNG Marine Incidents. In Proceedings of the CCPS Conference, Orlando, FL, USA, 29 June–1 July 2004; pp. 1–20.
65. Suardin, J.A.; Qi, R.; Cormier, B.R.; Rana, M.; Zhang, Y.; Mannan, M.S. Application of fire suppression materials on suppression of LNG pool fires. *J. Loss Prev. Process Ind.* **2011**, *24*, 63–75. [CrossRef]
66. Luketa, A.; Blanchat, T. The phoenix series large-scale methane gas burner experiments and liquid methane pool fires experiments on water. *Combust. Flame* **2015**, *162*, 4497–4513. [CrossRef]
67. *BS EN ISO 23306*; 2020 BSI Standards Publication Specification of Liquefied Natural Gas as a Fuel for Marine Applications. The British Standards Institution: London, UK, 2020.
68. Pio, G.; Ruocco, C.; Palma, V.; Salzano, E. Detailed kinetic mechanism for the hydrogen production via the oxidative reforming of ethanol. *Chem. Eng. Sci.* **2021**, *237*, 116591. [CrossRef]
69. Pio, G.; Dong, X.; Salzano, E.; Green, W.H. Automatically generated model for light alkene combustion. *Combust. Flame* **2022**, *241*, 112080. [CrossRef]
70. U.S. Environmental Protection Agency. *Handbook of Chemical Hazard Analysis Procedures*; Federal Emergency Management Agency Publications Office: Washington, DC, USA, 1988.
71. Cozzani, V.; Gubinelli, G.; Salzano, E. Escalation thresholds in the assessment of domino accidental events. *J. Hazard. Mater.* **2006**, *129*, 1–21. [CrossRef]
72. Muñoz, M.; Planas, E.; Ferrero, F.; Casal, J. Predicting the emissive power of hydrocarbon pool fires. *J. Hazard. Mater.* **2007**, *144*, 725–729. [CrossRef]
73. Carboni, M.; Pio, G.; Vianello, C.; Maschio, G.; Salzano, E. Large eddy simulation for the rapid phase transition of LNG. *Saf. Sci.* **2021**, *133*, 105001. [CrossRef]
74. Kim, B.K.; Ng, D.; Mentzer, R.A.; Sam Mannan, M. Key parametric analysis on designing an effective forced mitigation system for LNG spill emergency. *J. Loss Prev. Process Ind.* **2013**, *26*, 1670–1678. [CrossRef]